



Published in final edited form as:

*Bone*. 2008 December ; 43(6): 1067–1074. doi:10.1016/j.bone.2008.07.248.

## FLUORIDE EFFECTS ON BONE FORMATION AND MINERALIZATION ARE INFLUENCED BY GENETICS

M. Mousny<sup>1</sup>, S. Omelon<sup>2</sup>, L. Wise<sup>2</sup>, E. T. Everett<sup>4</sup>, M. Dumitriu<sup>2</sup>, D. P. Holmyard<sup>2</sup>, X. Banse<sup>1</sup>, J. P. Devogelaer<sup>5</sup>, and M. D Grynepas<sup>2,3</sup>

<sup>1</sup>Orthopaedic Research Laboratory, Cliniques Universitaires Saint-Luc, Catholic University of Louvain, Brussels, Belgium

<sup>2</sup>Samuel Lunenfeld Research Institute, Mount Sinai Hospital, Ontario, Canada

<sup>3</sup>Laboratory Medicine and Pathobiology, University of Toronto

<sup>4</sup>Department of Pediatric Dentistry and The Carolina Center for Genome Sciences, University of North Carolina, Chapel Hill, North Carolina, USA

<sup>5</sup>Arthritis Unit, Cliniques Universitaires Saint-Luc, Catholic University of Louvain, Brussels, Belgium

### Abstract

**Introduction**—A variation in bone response to fluoride (F<sup>-</sup>) exposure has been attributed to genetic factors. Increasing fluoride doses (0ppm, 25ppm, 50ppm, 100ppm) for three inbred mouse strains with different susceptibilities to developing dental enamel fluorosis (A/J, a “susceptible” strain; SWR/J, an “intermediate” strain; 129P3/J, a “resistant” strain) had different effects on their cortical and trabecular bone mechanical properties. In this paper, the structural and material properties of the bone were evaluated to explain the previously observed changes in mechanical properties.

**Materials and Methods**—This study assessed the effect of increasing fluoride doses on the bone formation, microarchitecture, mineralization and microhardness of the A/J, SWR/J and 129P3/J mouse strains. Bone microarchitecture was quantified with microcomputed tomography and strut analysis. Bone formation was evaluated by static histomorphometry. Bone mineralization was quantified with backscattered electron (BSE) imaging and powder x-ray diffraction. Microhardness measurements were taken from the vertebral bodies (cortical and trabecular bone) and the cortex of the distal femur.

**Results**—Fluoride treatment had no significant effect on bone microarchitecture for any of the strains. All three strains demonstrated a significant increase in osteoid formation at the largest fluoride dose. Vertebral body trabecular bone BSE imaging revealed significantly decreased mineralization heterogeneity in the SWR/J strain at 50ppm and 100ppm F<sup>-</sup>. The trabecular and cortical bone mineralization profiles showed a non-significant shift towards higher mineralization with increasing F<sup>-</sup> dose in the three strains. Powder x-ray diffraction showed significantly smaller crystals for the 129P3/J strain, and increased crystal width with increasing F<sup>-</sup> dose for all strains. There was no effect of F<sup>-</sup> on trabecular and cortical bone microhardness.

---

**Corresponding author:** Marc D. Grynepas, Samuel Lunenfeld Research Institute, Mount Sinai Hospital, Room 840, 600 University Avenue, Toronto, Ontario M5G 1X5, Canada, **Phone:** (416) 586-4464, **Fax:** (416) 586-1554, **Email:** grynepas@mshri.on.ca.

**Publisher's Disclaimer:** This is a PDF file of an unedited manuscript that has been accepted for publication. As a service to our customers we are providing this early version of the manuscript. The manuscript will undergo copyediting, typesetting, and review of the resulting proof before it is published in its final citable form. Please note that during the production process errors may be discovered which could affect the content, and all legal disclaimers that apply to the journal pertain.

**Conclusion**—Fluoride treatment had no significant effect on bone microarchitecture in these three strains. The increased osteoid formation and decreased mineralization heterogeneity support the theory that  $F^-$  delays mineralization of new bone. The increasing crystal width with increasing  $F^-$  dose confirms earlier results and correlates with most of the decreased mechanical properties. An increase in bone  $F^-$  may affect the mineral-organic interfacial bonding and/or bone matrix proteins, interfering with bone crystal growth inhibition on the crystallite faces as well as bonding between the mineral and organic interface. The smaller bone crystallites of the 129P3/J (resistant) strain may indicate a stronger organic/inorganic interface, reducing crystallite growth rate and increasing interfacial mechanical strength.

### Keywords

fluoride; bone quality; genetic susceptibility / resistance; hydroxyapatite crystals; mineralorganic interfacial bonding

## INTRODUCTION

Fluoride ( $F^-$ ) is a trace element that is incorporated into bone mineral during bone formation [1]. Fluoride substitutes for the hydroxyl group in hydroxyapatite, forming fluorapatite. The action of fluoride on bone has been extensively studied and this ion has been shown to have an effect on bone mineral, bone cells and bone architecture [1]. The dose-dependent effects on mechanical properties are well-known, but the underlying mechanisms are still not fully understood. Furthermore, dose level alone is not the only factor affecting bone quality; the role of genetic factors has been emphasized in some epidemiological and clinical studies. Previous studies provide evidence of human non-responder populations to  $F^-$  [2] while some populations seem to be very sensitive to  $F^-$  at a wide range of doses [3,4,5,6,7]. Three inbred strains of mice (A/J, SWR/J, 129P3/J) that displayed variations in the onset and severity of dental/enamel fluorosis with equivalent  $F^-$  exposure [8], were shown to have different reductions in bone mechanical properties with equivalent  $F^-$  concentrations in their mineralized tissues [9]. The bone mechanical properties were reduced in the “susceptible strain” (A/J), moderately altered in the “intermediate strain” (SWR/J) and unaffected in the “resistant strain” (129P3/J), suggesting a genetic contribution to the variation in bone response to  $F^-$  content.

The purpose of this study was to assess the effects of increasing  $F^-$  doses on bone properties at the microscopic level (architecture, geometry, histology) and on bone mineralization, crystallite size and microhardness for the A/J, SWR/J and 129P3/J mouse strains in order to determine a possible mechanism for the previously reported differences in bone mechanical properties caused by  $F^-$  exposure.

## MATERIALS AND METHODS

### Animal husbandry

**Mice**—The bones used in this study were obtained from mice used for a previous study [9]. These were weanling (3-week-old) male mice from A/J, SWR/J, and 129P3/J inbred strains obtained from The Jackson Laboratory (Bar Harbor, ME). These three strains were selected because of differences in susceptibility to develop dental fluorosis (A/J is a “susceptible” strain, SWR/J is an “intermediate” strain and 129P3/J is a “resistant” strain) [8] as well as a varied response of bone mechanical properties to fluoride exposure [9]. This study was approved by the Indiana University School of Dentistry IACUC and all mice were housed within the Indiana University School of Dentistry Bioresearch Facility, an AAALAC-accredited unit. Mice were contained in boxed caging and allowed food and water *ad libitum*. They were fed a laboratory rodent diet (#5001, PMI® Nutrition International, Richmond, IN) that contained, by dry weight, 0.95% calcium, 0.67% phosphorus, 4.5IU/g vitamin D3, and 18ppm fluoride.

**Fluoride Treatment**—The deionized water was tested from multiple sites within the IUSD Bioresearch Facility and showed [F] ion =  $0.02 + 0.01$  ppm. NaF was used to raise the [F] ion to 25ppm, 50ppm and 100ppm. Four levels of fluoride (0, 25, 50 and 100ppm F<sup>-</sup>) were thus delivered in the drinking water as NaF from 3 weeks of age, for a period of 42 days. Deionized and fluoridated water was periodically analyzed by ion specific electrode (ISE) for fluoride concentration. Each batch of prepared 25ppm, 50ppm, and 100ppm water for the study was used only if the fluoride was within 4% of the target concentration. Each treatment group consisted of 6 mice, except for the A/J (25ppm), A/J (50ppm) and 129P3/J (100ppm) groups which consisted of 7 mice. At the end of the F<sup>-</sup> treatment, the mice were humanely euthanized. Selected bones were harvested for analysis.

## Design of experiment

**Preparation of Bones**—The lumbar vertebral bodies (VB) and femora (F) were dissected and kept moist with saline solution during preparation. They were stored at  $-20^{\circ}\text{C}$ .

**Strut analysis**—Distal thoracic vertebral bodies were used for strut analysis. Each vertebra was cleaned and trimmed to leave only the vertebral body. They were fixed in 10% neutral buffered formalin for one week. Samples were then dehydrated in ascending concentrations of acetone and subsequently infiltrated in ascending ratios of unpolymerized Spurr resin and acetone. The bones were finally embedded in blocks of Spurr resin that was polymerized in a  $60^{\circ}\text{C}$  oven for 48 hours. Several 5-micron thick coronal sections were then cut from each sample, using an automatic Reichert-Jung 2500 rotary microtome (Leica Microsystems). Sections were placed on gelatinized slides and incubated in a  $60^{\circ}\text{C}$  oven for 48 hours, then stained with Von Kossa and imaged using light microscopy. Trabecular bone area was analyzed using the Quantimet 570 (Leica) image processing and analysis system. The connectivity was evaluated by skeletonizing the image of trabecular bone, representing the trabeculae as struts. Nodes represented points at which three or more struts were connected. The number of nodes (NN;mm<sup>-2</sup>) was determined as a measure of connectivity, and the number of free ends (NFE;mm<sup>-2</sup>) was determined as a measure of disconnectivity [10].

**Microcomputed tomography of thoracic vertebral bodies**—Thoracic vertebral bodies were scanned using microcomputed tomography ( $\mu\text{CT}$ ) to evaluate the trabecular bone architecture (Figure 1). These vertebrae were embedded in microtubes using epoxy resin to eliminate movement during the scan.  $\mu\text{CT}$  was performed using a desktop  $\mu\text{CT}$  with a  $6.5\ \mu\text{m}$  voxel size (GE Medical Systems eXplore Locus SP Specimen Scanner, London, Ontario, Canada). Scans were reconstructed and calibrated using a hydroxyapatite standard. Final images and 3D volumes were analyzed using MicroView CT visualization software (GE Medical Systems, London, Ontario, Canada). Each vertebral body was cropped out of the reconstructed volume and rotated so that the mediolateral axis coincided with the x-axis. The region of interest (trabecular bone) was then defined in each vertebral body 3D image and analyzed to determine the following trabecular bone parameters: bone volume fraction (BVF=Bone Volume/Total Volume; %), bone surface area (SA; mm<sup>2</sup>), mean trabecular thickness (TbTh;  $\mu\text{m}$ ), trabecular number (TbN; mm<sup>-1</sup>), and mean trabecular separation (TbSp;  $\mu\text{m}$ ). The structure model index (SMI) was also determined. SMI gives information about the curvature of the surface and estimates how “plate-like” or “rod-like” a trabecular structure is. A SMI value of zero indicates bone architecture with “plates” while a SMI value of 3 is an indicator of “rods”. Anisotropy was analyzed by determining the ratio between the length of one axis versus another (a1/a3, a1/a2, a2/a3). This allowed us to determine the degree of symmetry and orientation of the trabecular structure: the closer the ratio is to 1, the less anisotropic the sample.

**Static histomorphometry**—Coronal sections at midpoint of the embedded vertebral bodies used for strut analysis were stained with Goldner's trichrome, resulting in blue/green staining of mineralized bone and red/orange staining of osteoid [11]. Trabecular bone was analyzed using a 25x objective lens (Zeiss) connected to a video camera (Retiga 1300). The total trabecular area was analyzed as serial fields using the Leitz Bioquant morphometry system (Bioquant Nova Prime, Version 6.50.10). We determined the following static histomorphometric parameters: trabecular bone volume (BV/TV; %; ratio between trabecular bone volume and tissue volume), mineralized trabecular bone volume (Mdv/TV; %; ratio between mineralized trabecular bone volume and tissue volume), osteoid volume (OV/BV; %; ratio between osteoid volume and bone volume), osteoid surface (OS/BS; %; ratio between total osteoid surface and bone surface) and osteoid thickness (OTh;  $\mu\text{m}$ ).

**Backscattered electron imaging**—Following three-point bending of right femora, as reported in a previous study [9], the distal end of the broken femur was embedded in Spurr blocks, using the same procedure as described for the vertebral bodies. The embedded femora as well as the Spurr-embedded blocks of thoracic vertebral bodies were used for evaluation of mineralization distribution using backscattered electron (BSE) imaging. Blocks were cut, polished, carbon-coated and imaged using backscattered electron (BSE) imaging (solid state BSE detector, FEI Company, Hillsboro, OR, USA) on a Philips XL30 ESEM (FEI). The relative backscattering of the mineralized tissues was determined by comparison with a silicon dioxide standard, which was measured between every specimen. Histograms of the grey level distribution were created for the trabecular bone of the vertebral bodies and for the distal femur cortex. Increasing brightness corresponds with increasing mineralization [12]. From the histogram, the grey level of the histogram peak was determined and used to represent the overall degree of mineralization. The full width at half the maximum height (FWHM) of the histogram represents the heterogeneity of the mineralization distribution, and gives an approximation of the distribution of less-mineralized (younger) and more mineralized (older) bone.

**Powder x-ray diffraction/apatite crystallite size**—Powder x-ray diffraction was performed on bone powder, produced from left femora that were previously used to determine femur fluoride concentration [9]. The powder was prepared as follows: Bones were manually crushed, tri-washed and lyophilized for 48 hours. A 2:1 chloroform:methanol solution was used to defat the specimens overnight [13]. The solution was decanted and replaced with methanol. After one hour, the methanol was decanted and the specimens dried at ambient temperature. Dry specimens were ground to a powder ( $< 45 \mu\text{m}$  particle size) using a cryogenic freezer mill (SPEX Certiprep 6750 Freezer Mill).

The bone powder specimens and a NIST standard reference material (2910, Calcium Hydroxyapatite) were scanned from  $24.5$  to  $27.0$   $^{\circ}2\theta$  at a scan speed of  $0.1$   $^{\circ}2\theta/\text{min}$  and  $37.0$  to  $42.0$   $^{\circ}2\theta$  at a scan speed of  $0.05$   $^{\circ}2\theta/\text{min}$  (step size  $0.004$   $^{\circ}2\theta$ ,  $40$  kV,  $30$  mA, Cu  $K_{\alpha}$  radiation, Rigaku MultiFlex, Rigaku/MSO, The Woodlands, TX, USA). All specimens were remounted and re-scanned for a total of 3 scans/specimen. Crystallite size was calculated from the peak broadening of the powder x-ray diffraction peaks [14].

Peak broadening is quantified with the “full width at half the maximum height” (FWHM) of the peak ( $\beta_{1/2}$ ), which is composed of broadening caused by both the specimen and the instrument. The FWHM of the  $26$   $^{\circ}2\theta$  peak ((002) plane-hydroxyapatite crystal length) and  $40$   $^{\circ}2\theta$  peak ((310) plane-hydroxyapatite crystal cross-section or width) were quantified with the profile fitting function of Jade (XRD pattern processing software, v. 6.5, Materials Data Inc.). The FWHM due to the instrument (instrument broadening ( $\beta_i$ )), was measured by scanning reference silicon at  $26$  and  $55$   $^{\circ}2\theta$ . The broadening due to the specimen only (corrected  $\beta_{1/2}$ ) was calculated from the square root of the instrument broadening squared subtracted from the

measured specimen peak broadening squared. This corrected  $\beta_{1/2}$  was used to calculate the crystalline size between the (002) and the (310) planes using the Scherrer equation,

$$D = \frac{57.3 K \lambda}{\beta_{1/2} \cos(\theta)}$$

where 57.3 is a conversion factor from degrees to radians, K is a correction factor (0.9) used to reflect the elongated apatite crystals of bone,  $\lambda$  is the K-emission wavelength of copper,  $\theta$  is the diffraction angle, and D is the size of the crystallite in angstroms along the specific axis. The means of three independent FWHM values for each 26 and 40 °2 $\theta$  peak were calculated for each specimen.

**Cortical and trabecular microhardness**—After the BSE study was complete, microhardness measurements of the Spurr-embedded thoracic vertebral bodies and distal femora were performed. The microhardness of trabecular bone (coronal surface of vertebral bodies) and cortical bone (coronal plane of vertebral body cortical shell and axial surface of distal femora) was determined by using a microhardness testing machine (Mitutoyo HM-122, S/N 260113). Microhardness testing consists of measuring the resistance of bone to indentation. During the test, a pyramidal diamond indenter of known geometry was lowered onto the sample under a known load for 10 seconds, leaving an indentation on its surface. The depth of the indentation is related to the hardness of the bone. Given that the diamond is pyramidal, there is a linear relationship between the length of the indentation and the depth. Length can therefore be used as a proxy measure for depth. The indentation length and the load are used to calculate the hardness of the bone, using this equation:

$$Hv = k \frac{F}{S} = 0.102 \frac{F}{S} = 0.102 \frac{2F \sin \frac{\theta}{2}}{d^2} = 0.1891 \frac{F}{D^2}$$

Where *HV* is the Vickers Hardness, *k* is a constant ( $k = \frac{1}{g} = \frac{1}{9.8} \cong 0.102$ , where *g* is the standard acceleration due to gravity), *F* is the test force (0.025kg), *S* is the surface area of indentation (mm<sup>2</sup>), *d* is the average length of two diagonals (mm), and  $\theta$  is the face-to-face apex angle of diamond indenter (136°). Ten measures were performed for each type of bone (trabecular/cortical) for each sample and the average of these ten measures was calculated.

### Statistical analysis

Statistical analysis was performed using SPSS (version 12.0) (SPSS Inc., Chicago IL) software. Two-way Analysis of Variance (ANOVA, general linear model) was used to compare the effects of F<sup>-</sup> treatment and genetic strain on the bone properties. Post hoc multiple comparisons between the three strains and four fluoride treatments were performed using the Bonferroni test. The correlation between the crystallite width and mechanical properties for each strain was made with the bivariate correlation function (SPSS) with a two-tailed Pearson coefficient. A p value of  $\leq 0.05$  was required to consider a difference significant. A confidence level of 90% ( $p < 0.1$ ) indicated a statistical trend. Data are presented as mean  $\pm$  SD.

## RESULTS

### Strut analysis

There were no significant changes in the thoracic VB trabecular bone connectivity with fluoride treatment in the three strains (Table 1).

### Microcomputed tomography of thoracic vertebral bodies

Analysis of the trabecular bone parameters (BVF, SA, TbTh, TbN and TbSp) did not show any significant differences between the groups (Table 1). No statistical differences were observed between SMI values (Table 1). Anisotropy analysis (a1/a3, a1/a2, a2/a3) did not show any significant change with fluoride treatment within the three strains (Table 1).

### Static histomorphometry

The only significant histomorphometric differences observed were in osteoid formation (Table 2). There was an increase in osteoid volume and osteoid surface between the control and the 100ppm groups for all three strains. The increase observed in osteoid thickness was statistically significant for the 129P3/J strain. The percent increase in osteoid volume for the three strains correlated with their susceptibility to dental fluorosis, with a 26-fold increase for the A/J strain, a 7-fold increase for the SWR/J and a 6-fold increase for the 129P3/J strain. The osteoid surface followed a similar trend, with a 46-fold increase for the A/J, a 5-fold for the SWR/J and a 4-fold increase for the 129P3/J strain. This trend also applied to osteoid thickness, with a 4-fold increase for the A/J, a 2-fold increase for the SWR/J and a 1.3-fold increase for the 129 P3/J strain. The comparison of the three strains for each fluoride dose treatment showed that the osteoid volume and surface were significantly larger in the 129P3/J strain ( $p \leq 0.05$ ).

### Backscattered electron imaging

The average peak grey level of femur cortical bone increased with fluoride treatment, but the observed differences were not statistically significant (Table 3). Grey levels increased by 2% in the A/J strain, by 8% in the SWR/J strain and by 12% in the 129P3/J strain at 100ppm  $F^-$ . The FWHM did not demonstrate any significant changes in the three strains (Table 3).

While the average peak grey level of vertebral body trabecular bone increased with fluoride treatment, the observed differences were not statistically significant (Table 3). Grey level increased by 7% in A/J, by 20% in SWR/J and by 12% in 129P3/J (Table 3). While the FWHM decreased in the three strains with  $F^-$  treatment, these changes were only significant in the SWR/J (Table 3). The FWHM decreased by 4% in A/J, by 22% in SWR/J and by 21% in 129P3/J.

### X-ray diffraction study

A 2-way ANOVA analysis of the effect of genotype and fluoride dose on the crystal length (002) showed an effect of genotype on crystallite length, independent of fluoride dose. The crystallite length of the resistant (129P3/J) strain was significantly smaller than the same dimension for the other strains ( $p < 0.05$ ) (Table 4). The  $F^-$  treatment did not significantly affect the crystal length in any of the three strains.

A similar analysis for the crystallite width (310) showed an effect of both genotype and fluoride concentration, with no evidence of interaction between the two factors. The crystallite width of the 129P3/J strain was significantly smaller than for the A/J and SWR/J strains ( $p < 0.05$ ) (Table 4). All strains showed a significant increase in crystallite width between 0 and 100ppm  $F^-$  (Table 4). The susceptible strain A/J showed a 5.7% increase in crystallite width, the intermediate strain SWR/J showed a 10.6% increase and the resistant strain 129P3/J showed a 8% increase. At 100ppm  $F^-$  dose treatment, the crystallite width of the resistant strain 129P3/J was still significantly smaller than for the two other strains ( $p < 0.05$ ).

The correlation analysis between the crystallite width and mechanical properties (from a previous study [9]) for each strain at all  $F^-$  dose treatments showed that the crystallite width increase correlated with most of the decreased mechanical properties described in the susceptible (A/J) and intermediate (SWR/J) strains (Table 5, Figure 2).

### Cortical and trabecular bone microhardness

No statistically significant differences were observed between the microhardness values of the cortical or the trabecular bone between the three strains at any  $F^-$  concentration (Table 6).

## DISCUSSION

In our previous study [9], we showed that increasing doses of fluoride (0ppm, 25ppm, 50ppm, 100ppm) had different effects on the bone properties of three inbred mouse strains which demonstrated different susceptibilities to developing enamel fluorosis (A/J, a “susceptible” strain; SWR/J, an “intermediate” strain; 129P3/J, a “resistant” strain). Although significant increases of fluoride concentration in femora and vertebral bodies could be demonstrated, and no significant effects on bone macroarchitecture and bone mineral densities (BMD) were found in the three strains, mechanical testing showed significant degradation of bone mechanical properties in the A/J strain, whereas moderate degradation in the SWR/J strain and no effect in the 129P3/J strain were observed. We concluded that genetic factors may contribute to the variation in bone response to fluoride exposure and that the differences observed between the three strains could not be explained by an alteration of the bone macroarchitecture or by a different influence of fluoride on BMD. The purpose of this study was to determine if microarchitecture, histomorphometry, mineralization or microhardness were influenced by fluoride treatments and could be correlated with the previously observed reduction in bone mechanical properties.

Regarding bone microarchitecture, neither microcomputed tomography of thoracic vertebral body nor strut analysis showed any significant changes with fluoride treatment in the three strains. Fluoride therapy has been showed to increase trabecular thickness but to leave connectivity unaltered [15]. In our study, we did not find any change in vertebral body connectivity or in trabecular thickness. The absence of significant changes may be explained by the fact that fluoride was administered for only 42 days, which may be too short a period of time to have any significant effect on trabecular thickness. Therefore the differences in bone mechanical properties observed for the A/J and SWR/J strains with fluoride treatment [9] cannot be explained by altered bone microarchitecture.

It is recognized that fluoride is usually not incorporated into fully-mineralized, mature bone and accumulates only in bone formed during the period of fluoride exposure [16]. This explains why fluoride concentration is generally higher in sites with a high turnover rate, such as cancellous rather than cortical bone. In our study, fluoride was given to young (that is, rapidly growing) mice and this explains the significant increases (concordant with increasing fluoride dose) of fluoride concentration observed in femora and vertebral bodies in all three strains [9]. As noted in our previous paper, we selected fluoride concentration in the water that would yield serum concentrations of  $\sim 8 \mu\text{mol/L}$  at 50ppm and  $\sim 12 \mu\text{mol/L}$  at 100ppm, which are greater than the plasma fluoride concentrations measured in humans when drinking water is optimally fluoridated ( $0.5\text{--}1.5 \mu\text{mol/L}$ ) [17], but which do correspond to the therapeutic range of fluoride for osteoporosis treatment ( $5\text{--}10 \mu\text{mol/L}$ ). High doses of fluoride were shown to affect bone cells and therefore remodeling processes. Fluoride has been shown to have a mitogenic effect on osteoblasts [18,19,20]. Effects of fluoride on osteoclasts have also been described [21], and fluoride effects on osteoclastogenesis have been demonstrated to be influenced by genetic background [22]. The cumulative result of these effects is a net increase in bone formation. This is consistent with our observations of osteoid formation in all three mouse strains; the osteoid formation was the only parameter that showed significant changes. In all three strains, we noted a significant increase in osteoid formation at the largest fluoride dose. The percent increase in osteoid volume, surface and thickness for the three strains correlated with their susceptibility to dental fluorosis, but the overall osteoid formation was significantly larger in the 129P3/J strain

Fluoride has also been shown to have an effect on mineralization. It retards mineralization and the mineral produced is less susceptible to dissolution [23,24,25]. Alterations in bone crystal structure have also been described [24]. In our study, the BSE mineralization profile of cortical and trabecular bone showed a non-significant increase towards higher mineralization with increasing  $F^-$  dose in the three strains. This is consistent with the increased resistance to dissolution of bone mineral with an increased fluoride content. Fluoride treatment had different effects on mineralization heterogeneity of the trabecular and cortical bone. We observed a decrease in mineralization heterogeneity in the trabecular bone, which was consistent with observations that fluoride delays mineralization of new bone. The absence of an effect on cortical bone mineralization heterogeneity may be explained by site-specific differences in bone turnover, as there is a higher turnover in trabecular bone.

It remains unclear if the substitution of fluoride ions for hydroxyl ions affects the size of the crystallites. Most authors accept that the crystal length is unchanged in  $F^-$  treatment [26,27]; however there remains debate about changes in crystal width. Some authors described an increase in crystal width [26,28,29], while others found no significant changes [27]. In this study, we observed a significant increase in crystal width at the largest  $F^-$  dose for all three strains. This relative increase in crystal width was similar in the three strains. However the absolute crystal size (length and width) was also inherently different between the strains. The 129P3/J (“resistant”) strain had smaller crystals in both measured dimensions than the other strains for all fluoride doses. The overall smaller crystal size suggests that the crystal growth rate of the resistant strain is slower than that of the other strains. This reduced crystal growth rate may be due to different mineral-collagen interface conditions that reduce the flux of calcium and phosphate ions to the apatite crystal surface.

We found a correlation between the crystallite width increase and most of the observed decreased mechanical properties in the A/J and SWR/J strains (Table 5, Figure 2). These observations suggest that bone crystal size may play an important role in determining bone quality. The fact that the 129P3/J resistant strain has the strongest bone and the smallest bone crystal may suggest that these mice have a stronger mineral-organic interfacial bonding, which has previously been shown to play an important role in bone quality [30]. The quality of the mineral-organic interfacial bonding and/or bone matrix proteins could therefore be influenced by genetics, and the observed differences between the three strains may be explained by different genetic factors whose specific action is still not known.

To test bone mechanical properties at the microscopic level, we performed a microhardness study of trabecular bone (thoracic vertebral body) and cortical bone (thoracic vertebral body and distal femur). This test has the theoretical advantage of eliminating architectural considerations, instead focusing on the tissue-level mechanical properties of the bone. In our study, we did not find statistically significant  $F^-$  induced changes in trabecular and cortical bone microhardness for any of the three strains. These results may be influenced by the lack of precision of this test. Variations in trabecular shape, orientation and number, as well as variations in mineral distribution and properties throughout individual trabeculae, are known to influence the results of this test [31]. This lack of precision is also present in cortical bone microhardness study, as we tested femur and VB cortical bone microhardness at one cross-section only. The absence of any change in microhardness may also be explained by the short period of fluoride treatment and by the fact that  $F^-$  was given to rapidly growing mice. Therefore we cannot draw any certain conclusions from the absence of significant differences in the results.

In conclusion, fluoride is known to have biological effects on bone cells, as well as chemical and physical effects on bone crystals. In the present study, fluoride treatment had no effect on bone microarchitecture in the three strains. The increased osteoid formation and decreased

mineralization heterogeneity support the theories that  $F^-$  stimulates osteoblastic activity and delays mineralization of new bone. The 129P3/J resistant strain was shown to have smaller bone crystals and a correlation was found between the  $F^-$  induced increase in crystal width and most of the decreased mechanical properties. Interfacial bonding interactions between the mineral and organic phases of bone have been shown to play an important role in bone mechanical properties [32], and different types of interaction have been described [33,34,35, 36,37]. In Figure 3, we propose a model that could explain the effect of mineral-collagen interface quality and fluoride concentration on crystal growth and composite material strength. At low fluoride dose (Figure 3, a and b), the 129P3/J resistant strain has a stronger organic-inorganic interface than the strains A/J and SWR/J. This strong interfacial bonding may reduce crystallite growth rate, explaining the smaller bone crystals discovered in the 129P3/J strain, and may increase the composite material strength. *In vitro* studies have demonstrated that fluoride ions could alter bone mechanical properties by altering mineral-organic interfacial bonding [32,38,39]. At high fluoride dose (Figure 3, c and d), such interfacial bonding alteration could weaken the mineral-organic bond and reduce interfacial mechanical strength. The weaker mineral-organic interface allows an increased flux of calcium and phosphate ions to the apatite crystal surface, which explains the increased crystal width observed in the three strains. This increase in crystal width was similar in the three strains and the resistant 129P3/J strain had still the smallest bone crystals at high fluoride dose, which may explain the absence of bone mechanical properties alteration in this strain.

Another possible mechanism of fluoride action would be an alteration of bone matrix proteins, i.e. collagen and noncollagenous proteins. Collagen and noncollagenous proteins are of significant importance for the biomechanical integrity of the bone [31,40,41,42,43] and many bone matrix proteins play important roles in mineralization [44]. Miao *et al.* [45] have investigated the effects of fluoride treatment (221 mg/L NaF in drinking water for two months) on rat calvarial osteoblasts. They showed that excessive fluoride intake could inhibit the synthesis of type I collagen and decrease the degree of collagen cross-linking. An influence of fluoride on proteoglycan structure synthesized by mineralizing bone cells [46] and on expression of matrix metalloproteinases [47] has also been proposed. Kindt *et al.* (39) showed that enhanced formation of superficial fluoroapatite weakened the protein-hydroxyapatite interfaces but NaF was also found to be a potent agent for extracting noncollagenous proteins from bone powder. It must be pointed out that these effects were demonstrated in *in vitro* studies and that they may be different *in vivo*.

Bone quality is thus a complex property that we do not fully understand, and the way the fluoride alters bone quality is still unclear. Possible mechanisms would be an alteration of mineral-organic interfacial bonding and/or an effect on bone matrix proteins. The present study also emphasizes the importance of considering bone mineral crystal size, mineral-organic interfacial bonding and bone matrix proteins in understanding bone quality. This has an important clinical impact, as alterations in bone collagen quality has been observed with aging [48].

## ACKNOWLEDGEMENTS

We thank Ms C. Benoit, Ms K. Tupy, Ms. D. Faust and Mr. R. Cheung for their technical assistance during this study. This work was funded by a grant from the Willy & Marcy De Vooght Foundation as well as a grant from the Zimmer Society, and by a NIH/NIDCR grant (DE014853) to ETE.

**Funding sources:** grant from the Willy & Marcy De Vooght Foundation grant from the Zimmer Society NIH/NIDCR (DE014853) to ETE.

## REFERENCES

1. Gryn timer, MD.; Chachra, D.; Limeback, H. The action of fluoride on bone. In: Henderson, JE.; Goltzman, D., editors. *The Osteoporosis Primer*. Cambridge University Press; 2000.
2. Dequeker J, Declerck K. Fluor in the treatment of osteoporosis. An overview of thirty years clinical research. *Schweiz Med Wochenschr/Journal Suisse de Medecine* 1993;123:2228–2234.
3. Russel AL. Dental fluorosis in Grand Rapids during the seventeenth year of fluoridation. *J Am Dent Assoc* 1962;65:608–612. [PubMed: 13975635]
4. Butler WJ, Segreto V, Collins E. Prevalence of dental mottling in school-aged lifetime residents of 16 Texas communities. *Am J Public Health* 1985;75:1408–1412. [PubMed: 4061713]
5. National Research Council. *Health effects of ingested fluoride*. USA: National Academy Press; 1993.
6. Yoder KM, Mabelya L, Robison VA, Dunipace AJ, Brizendine EJ, Stookey GK. Severe dental fluorosis in a Tanzanian population consuming water with negligible fluoride concentration. *Community Dentistry & Oral Epidemiology* 1998;26:382–393. [PubMed: 9870537]
7. Choubisa SL, Choubisa L, Choubisa DK. Endemic fluorosis in Rajasthan. *Indian J Environ Health* 2001;43:177–189. [PubMed: 12395525]
8. Everett ET, McHenry MAK, Reynolds N, Eggertsson H, Sullivan J, Kantman C, Martinez-Mier EA, Warrick JM, Stookey GK. Dental fluorosis : variability among different inbred strains. *J Dent Res* 2002;81:794–798. [PubMed: 12407097]
9. Mousny M, Banse X, Wise L, Everett ET, Hancock R, Vieth R, Devogelaer JP, Gryn timer MD. The genetic influence on bone susceptibility to fluoride. *Bone* 2006;39:1283–1289. [PubMed: 16920415]
10. Compston JE, Garrahan NJ, Croucher PI, Wright CD, Yamaguchi K. Quantitative analysis of trabecular bone structure. *Bone* 1993;14:187–192. [PubMed: 8363855]
11. Parfitt AM, Drezner MK, Glorieux FH, Kanis JA, Malluche H, Meunier PJ, Ott SM, Recker RR. Bone histomorphometry: standardization of nomenclature, symbols, and units. Report of the ASBMR Histomorphometry Nomenclature Committee. *J Bone Miner Res* 1987;2:595–610. [PubMed: 3455637]
12. Boyde A, Jones SJ. Back-scattered electron imaging of skeletal tissues. *Metab Bone Dis Relat Res* 1983;5:145–150. [PubMed: 6676627]
13. Burr DB, Miller L, Gryn timer M, Li J, Boyde A, Mashiba T, Hirano T, Johnston CC. Tissue mineralization is increased following 1-year treatment with high doses of bisphosphonates in dogs. *Bone* 2003;33:960–969. [PubMed: 14678856]
14. Klug, H.; Alexander, L. *X-ray diffraction procedures for polycrystalline and amorphous materials*. New York: Wiley; 1974.
15. Aaron JE, de Vernejoul MC, Kanis JA. Bone hypertrophy and trabecular generation in Paget’s disease and in fluoride-treated osteoporosis. *Bone Miner* 1992;17:399–413. [PubMed: 1623333]
16. Boivin G, Meunier PJ. Effects of fluoride on bone mineral. *Res. Clin. Forums* 1993;15:13–19.
17. Whitford, GM. *The metabolism and toxicity of fluoride*. In: Myers, HM., editor. Vol. 2nd ed.. Basel: Karger; 1996.
18. Boivin G, Chavassieux P, Chapuy MC, Baud CA, Meunier PJ. Skeletal fluorosis : histomorphometric analysis of bone changes and bone fluoride content in 29 patients. *Bone* 1989;10:89–99. [PubMed: 2765315]
19. Gruber HE, Baylink DJ. The effects of fluoride on bone. *Clin Orthop* 1991;267:264–277. [PubMed: 2044288]
20. Chavassieux P, Boivin G, Serre CM, Meunier PJ. Fluoride increases rat osteoblast function and population after in vivo administration but not after in vitro exposure. *Bone* 1993;14:721–725. [PubMed: 8268046]
21. Okuda A, Kanehisa J, Heersche JN. The effects of sodium fluoride on the resorptive activity of isolated osteoclasts. *J Bone Miner Res* 1990;5:S115–S120. [PubMed: 2339620]
22. Yan D, Gurumurthy A, Wright M, Wayne Pfeiler T, Loba EG, Everett ET. Genetic background influences fluoride’s effect on osteoclastogenesis. *Bone* 2007;41:1036–1044. [PubMed: 17936699]
23. Tenenbaum HC, Richards J, Holmyard D, Mamujee H, Gryn timer MD. The effect of fluoride on osteogenesis in vitro. *Cell & Materials* 1991;1:317–327.

24. Grynblas MD. Fluoride effects on bone crystals. *J Bone Miner Res* 1990;5:S169–S175. [PubMed: 2187325]
25. Grynblas MD, Rey C. The effect of fluoride treatment on bone mineral crystals in the rat. *Bone* 1992;13:423–429. [PubMed: 1476820]
26. Posner AS, Eanes ED, Harper RA, Zipkin I. X-ray diffraction analysis of the effect of fluoride on human bone apatite. *Arch Oral Biol* 1963;8:549–570. [PubMed: 14047596]
27. Grynblas, MD.; Simmons, ED.; Pritzker, KPH.; Hancock, RV.; Harrison, JE. Is fluoridated bone different from non-fluoridated bone?. In: Yousuf, S. Ali, editor. *Cell mediated calcification and matrix vesicles*. New York: Elsevier; 1986. p. 409-414.
28. Eanes ED, Meyer JL. The influence of fluoride on apatite formation from unstable supersaturated solutions at pH 7.4. *J Dent Res* 1978;57:617–624. [PubMed: 30787]
29. Chachra D, Turner CH, Dunipace AJ, Grynblas MD. The effect of fluoride on bone mineral in rabbits. *Calcif Tissue Int* 1999;64:345–351. [PubMed: 10089229]
30. Walsh WR, Guzelsu N. Mineral-organic interfacial bonding and the mechanical properties of cortical bone tissue. *Biomimetics* 1993;1:199–217.
31. Boskey AL, Wright TM, Blank RD. Collagen and bone strength. *J Bone and Miner Res* (14) 1999:330–335. [PubMed: 10027897]
32. Walsh WR, Guzelsu N. The role of ions and mineral-organic interfacial bonding on the compressive properties of cortical bone. *Biomed Mater Eng* 1993;3:75–84. [PubMed: 8369729]
33. Benardi G, Giro M, Gaillard C. Chromatography of polypeptides and proteins on hydroxyapatite columns: some new developments. *Biochim Biophys Acta* 1972;278:409–420. [PubMed: 5085667]
34. Pearce EIF. Ion displacement following the adsorption of anionic macromolecules on hydroxyapatite. *Calcif Tiss Int* 1981;33:395–402.
35. Kamyshnyi AL. Adsorption of globular proteins on solid corners: certain physicochemical characteristics. *Russ J Phys Chem* 1981;55:319–330.
36. Chander S, Fuerstenau DW. On the dissolution and interfacial properties of hydroxyapatite. *Colloids and Surfaces* 1982;4:101–120.
37. Boskey AL. Mineral-matrix interactions in bone and cartilage. *Clin Orthop Rel Res* 1992;281:244–274.
38. Walsh WR, Guzelsu N. Compressive properties of cortical bone: mineral-organic interfacial bonding. *Biomaterials* 1994;15:137–145. [PubMed: 8011860]
39. Kindt JH, Thurner PJ, Lauer ME, Bosma BL, Schitter G, Fantner GE, Izumi M, Weaver JC, Morse DE, Hansma PK. In situ observation of fluoride-ion-induced hydroxyapatite-collagen detachment on bone fracture surfaces by atomic force microscopy. *Nanotechnology* 2007;18:1–8.
40. Oxlund H, Barckman M, Ørtoft G, Andreassen TT. Reduced concentrations of collagen cross-links are associated with reduced strength of bone. *Bone* 1995;17:365S–371S. [PubMed: 8579939]
41. Wang X, Bank RA, Tekoppele JM, Hubbard GB, Atchanasiou KA, Agrawal CM. Effect of collagen denaturation on the toughness of bone. *Clin Orthop Rel Res* 2000;371:228–239.
42. Wang X, Bank RA, Tekoppele JM, Agrawal CM. The role of collagen in determining bone mechanical properties. *J Orthop Res* 2001;19:1021–1026. [PubMed: 11781000]
43. Burr DB. The contribution of the organic matrix to bone's material properties. *Bone* 2002;31:8–11. [PubMed: 12110405]
44. Young MF. Bone matrix proteins: their function, regulation and relationship to osteoporosis. *Osteoporos Int* 2003;14:535–542.
45. Miao Q, Xu M, Liu B, You B. In vivo and in vitro study on the effect of excessive fluoride on type I collagen of rats. *Wei Sheng Yen Chiu/Journal of Hygiene Research* 2002;31:145–147.
46. Waddington RJ, Langley MS. Structural analysis of proteoglycans synthesized by mineralizing bone cells in vitro in the presence of fluoride. *Matrix Biol* 1998;17:255–268. [PubMed: 9749942]
47. Waddington RJ, Langley MS. Altered expression of matrix metalloproteinases within mineralizing bone cells in vitro in the presence of fluoride. *Connect Tissue Res* 2003;44:88–95. [PubMed: 12745675]
48. Wang X, Shen X, Li X, Agrawal CM. Age-related changes in the collagen network and toughness of bone. *Bone* 2002;31:1–7. [PubMed: 12110404]

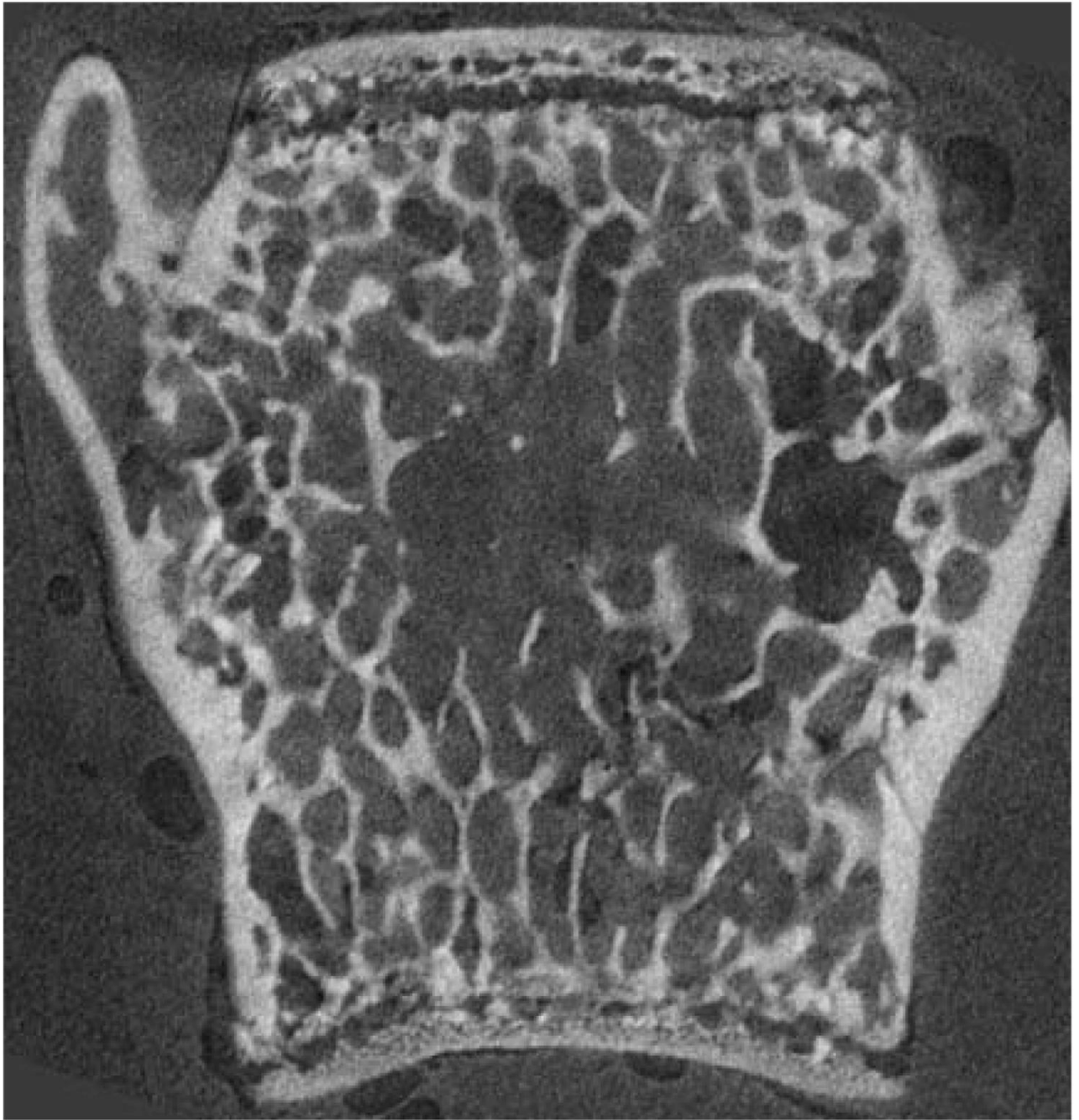


**Figure 1.**  
Coronal section of a thoracic vertebral body, obtained with microcomputed tomography.

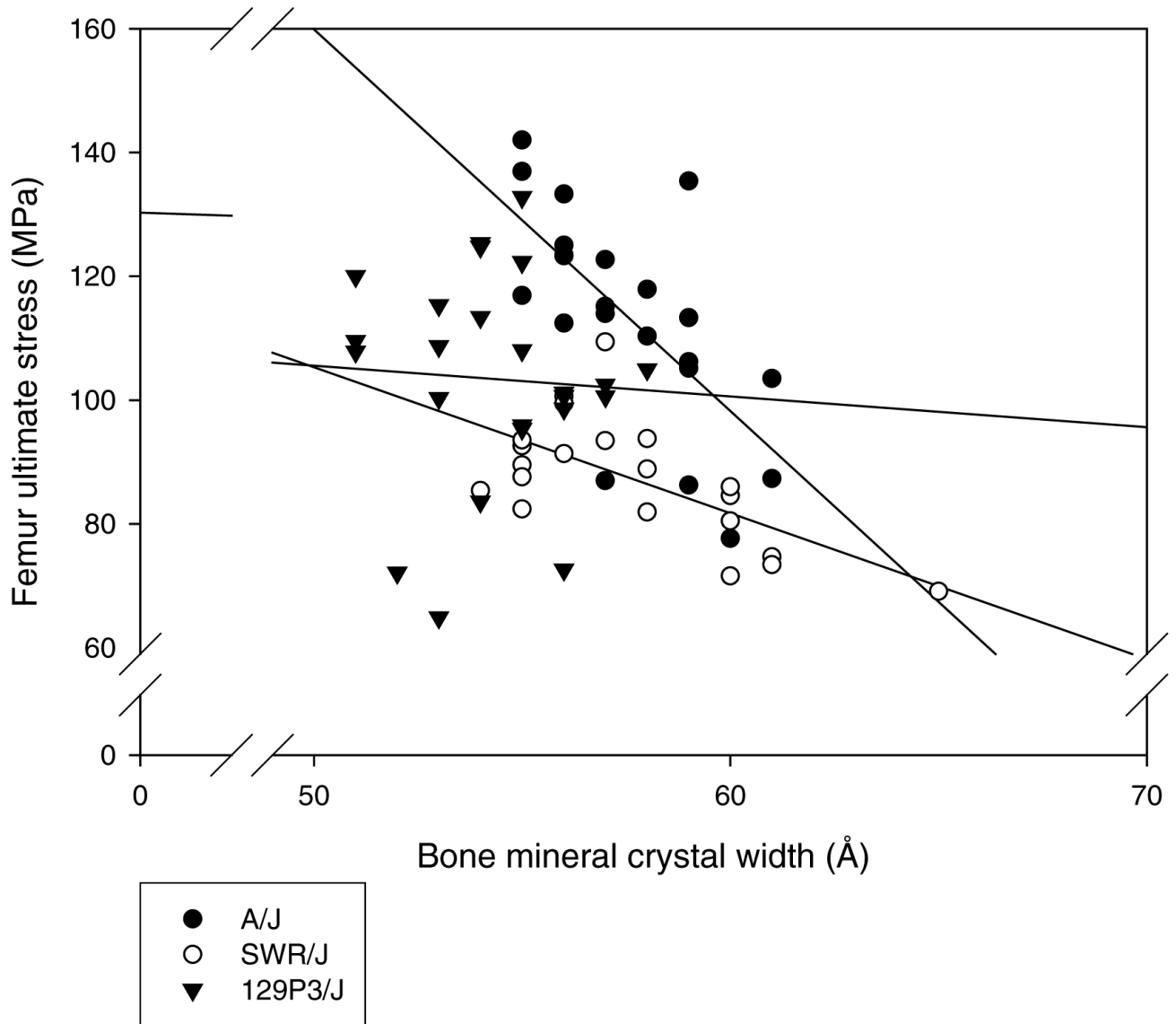


**Figure 2.** Correlation analysis between the crystallite width and femur ultimate stress for each strain at all  $F^-$  dose treatments. Crystallite width increase correlates with the decreased femur ultimate stress observed in the susceptible (A/J) and intermediate (SWR/J) strains.

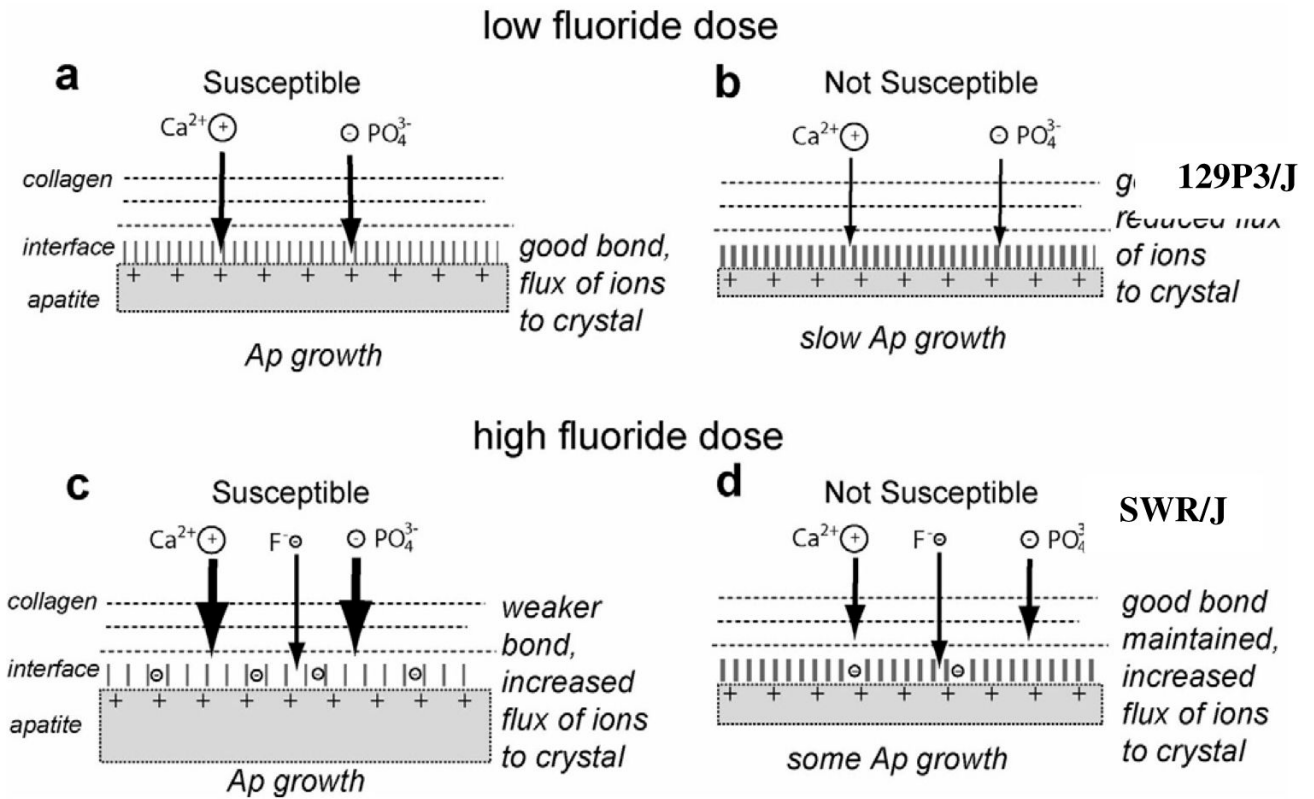


**Figure 3.** Schematic of the effect of mineral-collagen interface quality and fluoride concentration on crystal growth and composite material strength.

**TABLE 1**

Evaluation of thoracic vertebral body trabecular bone connectivity by strut analysis. Analysis of the number of free ends (NFE, disconnectivity) and of the number of nodes (NN, connectivity). Trabecular bone parameters (BVF, SA, TbTh, TbN and TbSp), SMI and anisotropy analysis of the thoracic vertebral body in the three strains.

	Fluoride Treatment (ppm)	Strain A/J	Strain SWR/J	Strain 129P3/J
NFE	0	39.67 ± 7.24	42.51 ± 12.83	38.05 ± 8.41
	100	39.25 ± 8.55	50.88 ± 7.09	47.08 ± 7.39
NN	0	10.24 ± 3.26	20.76 ± 3.80	25.36 ± 9.24
	100	7.25 ± 2.26	14.87 ± 5.71	24.36 ± 4.29
BVF (%)	0	0.22 ± 0.03	0.27 ± 0.03	0.30 ± 0.03
	100	0.20 ± 0.02	0.26 ± 0.02	0.27 ± 0.02
SA (mm <sup>2</sup> )	0	23.58 ± 2.94	27.68 ± 4.42	41.08 ± 4.18
	100	23.64 ± 6.45	28.63 ± 3.88	35.25 ± 7.22
Tb.Th. (μm)	0	0.026 ± 0.002	0.026 ± 0.004	0.028 ± 0.003
	100	0.024 ± 0.003	0.025 ± 0.002	0.027 ± 0.002
Tb.N. (mm <sup>-1</sup> )	0	8.66 ± 1.19	10.03 ± 0.98	10.66 ± 0.43
	100	8.55 ± 1.55	10.22 ± 0.83	9.92 ± 1.20
Tb.Sp. (μm)	0	0.091 ± 0.014	0.074 ± 0.008	0.066 ± 0.003
	100	0.097 ± 0.021	0.073 ± 0.007	0.075 ± 0.012
SMI	0	1.06 ± 0.40	0.47 ± 0.57	0.37 ± 0.35
	100	1.06 ± 0.38	0.69 ± 0.22	0.48 ± 0.28
a1/a3	0	1.73 ± 0.08	1.46 ± 0.07	1.52 ± 0.04
	100	1.51 ± 0.20	1.45 ± 0.09	1.55 ± 0.13
a1/a2	0	1.53 ± 0.07	1.37 ± 0.05	1.41 ± 0.06
	100	1.32 ± 0.17	1.35 ± 0.03	1.38 ± 0.13
a2/a3	0	1.13 ± 0.07	1.07 ± 0.04	1.08 ± 0.04
	100	1.14 ± 0.05	1.07 ± 0.05	1.12 ± 0.06

Data are presented as means ± SD. No significant statistical differences were noted.

**TABLE 2**

Histomorphometric analysis of the thoracic vertebral body in the three strains.

	Fluoride Treatment (ppm)	Strain A/J	Strain SWR/J	Strain 129P3/J
% Bone Volume of Tissue Volume BV/TV	0	11.48 ± 2.86	19.83 ± 3.15	24.65 ± 8.66
	25	12.55 ± 3.11	18.36 ± 3.54	24.50 ± 4.50
	50	13.58 ± 2.64	20.46 ± 4.72	23.69 ± 6.93
	100	12.85 ± 1.62	15.44 ± 2.89	24.43 ± 2.97
% Mineralized Bone of Tissue Volume MdV/TV	0	11.47 ± 2.84	19.83 ± 3.15	24.62 ± 8.64
	25	12.54 ± 3.11	18.35 ± 3.53	24.49 ± 4.50
	50	13.58 ± 2.64	20.45 ± 4.72	23.64 ± 6.93
	100	12.81 ± 1.62	15.43 ± 2.89	24.27 ± 2.94
% Osteoid Volume of Bone Volume OV/BV	0	0.01 ± 0.01	0.01 ± 0.02	0.11 ± 0.07
	25	0.02 ± 0.03	0.05 ± 0.05	0.05 ± 0.03
	50	0.04 ± 0.04	0.03 ± 0.03	0.20 ± 0.07
	100	0.26 ± 0.05 **	0.07 ± 0.03	0.64 ± 0.32 ***
% Osteoid Surface(OS/BS)	0	0.09 ± 0.19	0.22 ± 0.39	2.51 ± 1.65
	25	0.32 ± 0.45	0.54 ± 0.69	1.04 ± 0.83
	50	0.67 ± 0.59	0.40 ± 0.25	4.05 ± 1.18
	100	4.10 ± 0.91 ***	1.20 ± 0.54 *	9.40 ± 3.48 ***
Osteoid Thickness (mcm) OTh	0	0.38 ± 0.52	0.68 ± 0.76	1.24 ± 0.28
	25	0.31 ± 0.49	0.90 ± 0.72	1.16 ± 0.13
	50	0.94 ± 0.66	0.95 ± 0.53	1.40 ± 0.12
	100	1.37 ± 0.10	1.38 ± 0.25	1.61 ± 0.27 **

Data are presented as means ± SD.

A p value < 0.001 is noted as \*\*\*. A 0.001 < p < 0.05 is noted as \*\* and a 0.05 < p < 0.1 is noted as \*.

No significant statistical differences were noted for the BV/TV and mdV/TV, but there were significant differences in osteoid formation in the three strains.

**TABLE 3**

BSE analysis of distal femur cortical bone and thoracic vertebral body trabecular bone.

<b>BSE analysis of distal femur cortical bone</b>				
	<b>Fluoride Treatment (ppm)</b>	<b>A/J</b>	<b>SWR/J</b>	<b>129P3/J</b>
<b>Peak grey level</b>	0	212 ± 13	194 ± 14	190 ± 15
	25	200 ± 22	191 ± 12	215 ± 13
	50	201 ± 15	179 ± 19	210 ± 19
	100	216 ± 2	210 ± 12	212 ± 13
<b>FWHM</b>	0	44 ± 10	39 ± 9	44 ± 8
	25	36 ± 5	42 ± 7	39 ± 3
	50	38 ± 4	43 ± 10	43 ± 4
	100	46 ± 3	46 ± 4	45 ± 1
<b>BSE analysis of vertebral body trabecular bone</b>				
<b>Peak grey level</b>	0	181 ± 15	171 ± 23	165 ± 11
	25	170 ± 20	179 ± 24	171 ± 33
	50	176 ± 20	180 ± 24	178 ± 8
	100	193 ± 14	206 ± 18	185 ± 16
<b>FWHM</b>	0	55 ± 8	65 ± 6	62 ± 11
	25	57 ± 9	61 ± 6	62 ± 11
	50	49 ± 7	51 ± 7 <sup>***</sup>	53 ± 8
	100	53 ± 7	51 ± 6 <sup>***</sup>	48 ± 1 <sup>*</sup>

Data are presented as means ± SD.

A p value < 0.001 is noted as\*\*\*. A 0.001<p<0.05 is noted as \*\* and a 0.05<p< 0.1 is noted as \*.

For vertebral body trabecular bone, the fluoride dose significantly affected the full width of the half maximum value (FWHM) in the SWR/J strain.

**TABLE 4**

Bone mineral crystal length (002) and bone mineral crystal width (310), estimated by x-ray diffraction.

	Fluoride Treatment (ppm)	A/J	SWR/J	129P3/J
<b>Bone mineral crystal length (Å)</b>	0	147.2 ± 12.1	148.5 ± 5.9	130.4 ± 2.6
	25	140.3 ± 4.4	143.6 ± 9.4	135 ± 6.8
	50	146.7 ± 8.7	144.4 ± 10.6	133.5 ± 6.3
	100	141 ± 3.5	148.4 ± 10.5	133.9 ± 7.0
<b>Bone mineral crystal width (Å)</b>	0	56.2 ± 1.1	55.3 ± 1.4	52.2 ± 1.3
	25	56.2 ± 1.0	56.4 ± 1.1	53.5 ± 1.5
	50	58.5 ± 1.8 **	58.4 ± 2.1	54.5 ± 1.0 ***
	100	59.4 ± 1.1 ***	61.2 ± 2.2 ***	56.4 ± 1.0 ***

Data are presented as means ± SD.

A p value < 0.001 is noted as \*\*\*. A 0.001 < p < 0.05 is noted as \*\* and a 0.05 < p < 0.1 is noted as \*.

The fluoride treatment did not significantly affect the crystal length, but it induced a significant increase of the crystal width in all three strains. The crystal length and width were significantly smaller in the strain 129P3/J (p < 0.05), compared to the other two strains.

Statistical significance of the effect of  $F^-$  dose on mechanical properties between the 0 and 100ppm levels [9] and the Pearson Correlation Coefficient ( $r$ ) between the bone crystallite width (HA width) and the mechanical property for all  $F^-$  doses (2-tailed significance). NS: not statistically significant

The crystallite width increase correlated with most of the decreased mechanical properties described in the susceptible (A/J) and intermediate (SWR/J) strains.

TABLE 5

	A/J		SWR/J		129P3/J	
	$F^-$ dose	HA width	$F^-$ dose	HA width	$F^-$ dose	HA width
<b>Ultimate load</b>	$p < 0.001$	$r = -0.70$ ***	NS	$r = -0.56$ **	NS	NS
<b>F stiffness</b>	$0.001 < p < 0.05$	$r = -0.45$ **	NS	$r = -0.40$ *	NS	NS
<b>F ultimate stress</b>	$0.001 < p < 0.05$	$r = -0.67$ **	$0.001 < p < 0.05$	$r = -0.65$ **	NS	NS
<b>F modulus</b>	NS	NS	NS	$r = -0.47$ **	NS	NS
<b>VB ultimate load</b>	NS	$r = -0.48$ **	$p < 0.001$	$r = -0.68$ **	NS	NS
<b>VB stiffness</b>	$0.001 < p < 0.05$	$r = -0.40$ *	NS	NS	NS	NS
<b>VB ultimate stress</b>	NS	$r = -0.46$ *	$p < 0.001$	$r = -0.82$ ***	NS	NS
<b>VB modulus</b>	$0.001 < p < 0.05$	$r = -0.39$ *	NS	NS	NS	NS
<b>FN ultimate load</b>	$0.001 < p < 0.05$	$r = -0.72$ ***	$0.001 < p < 0.05$	$r = -0.61$ **	NS	NS
<b>FN stiffness</b>	NS	$r = -0.50$ **	NS	NS	NS	NS

**TABLE 6**

Microhardness of trabecular and cortical bone in vertebral bodies (VB), and of cortical bone in distal femurs in each treatment group.

	Fluoride Treatment (ppm)	Strain A/J	Strain SWR/J	Strain 129P3/J
<b>VB microhardness for trabecular bone</b>	<b>0</b>	27.6 ± 2.1	25.1 ± 2.5	25.9 ± 1.7
	<b>100</b>	24.5 ± 2.4	24.8 ± 3.2	25.6 ± 1.7
<b>VB microhardness for cortical bone</b>	<b>0</b>	31.1 ± 2.0	30.3 ± 0.9	31.7 ± 1.7
	<b>100</b>	31.4 ± 3.1	30.6 ± 1.6	31.4 ± 1.3
<b>Distal femur cortex microhardness</b>	<b>0</b>	39.4 ± 1.5	36.8 ± 2.3	37.9 ± 2.6
	<b>100</b>	38.0 ± 2.5	35.3 ± 1.0	37.5 ± 1.7

Data are presented as means ± SD. No statistical difference was noted for the microhardness of cortical and trabecular bone in the three strains.